Topological Node-Line Semimetal and Dirac Semimetal State in Antiperovskite Cu_3PdN

Rui Yu,[1] Hongming Weng,[2,3,*] Zhong Fang,[2,3] Xi Dai,[2,3] and Xiao Hu[1,†]
[1]*International Center for Materials Nanoarchitectonics (WPI-MANA), National Institute for Materials Science, Tsukuba 305-0044, Japan*
[2]*Beijing National Laboratory for Condensed Matter Physics and Institute of Physics, Chinese Academy of Sciences, Beijing 100190, China*
[3]*Collaborative Innovation Center of Quantum Matter, Beijing 100190, China*
(Received 22 April 2015; published 17 July 2015)

Based on first-principles calculation and effective model analysis, we propose that the cubic antiperovskite material Cu_3PdN can host a three-dimensional (3D) topological node-line semimetal state when spin-orbit coupling (SOC) is ignored, which is protected by the coexistence of time-reversal and inversion symmetry. There are three node-line circles in total due to the cubic symmetry. Drumheadlike surface flat bands are also derived. When SOC is included, each node line evolves into a pair of stable 3D Dirac points as protected by C_4 crystal symmetry. This is remarkably distinguished from the Dirac semimetals known so far, such as Na_3Bi and Cd_3As_2, both having only one pair of Dirac points. Once C_4 symmetry is broken, the Dirac points are gapped and the system becomes a strong topological insulator with (1;111) Z_2 indices.

DOI: 10.1103/PhysRevLett.115.036807 PACS numbers: 73.20.At, 71.55.Ak, 73.43.−f

Introduction.—Band topology in condensed-matter material has attracted broad interest in recent years. It has benefitted from the discovery of two-dimensional (2D) and three-dimensional (3D) topological insulators (TIs) [1,2]. These materials exhibit a bulk energy gap between the valence and conduction bands, similar to normal insulators, but with gapless boundary states that are protected by the band topology of bulk states. Topological classification has also been proposed for 3D metals [3]. The topological invariant, so called Fermi Chern number, can be defined on a closed 2D manifold, such as the Fermi surface, in 3D momentum space [3–5]. This is essentially the same as the Chern number defined in the whole 2D Brillouin zone for insulators. Up to now, three types of nontrivial topological metals have been proposed. They are the Weyl semimetal [6–9], Dirac semimetal [4,10], and node-line semimetal (NLS) [11,12]. All of them have band crossing points due to band inversion [13]. For Weyl and Dirac semimetals, the band crossing points, which compose the Fermi surface, are located at different positions. For the NLS, the crossing points around the Fermi level form a closed loop. The breakthrough in topological semimetal research happened in the material realization of the Dirac semimetal state in Na_3Bi and Cd_3As_2, which were first predicted theoretically [4,10] and then confirmed by several experiments [14–17]. Starting from the Dirac semimetal, one can obtain the Weyl semimetal by breaking either time-reversal [7,8,18] or inversion symmetry [19–22]. Among them, the prediction of the Weyl semimetal state in the nonmagnetic and noncentrosymmetric TaAs family [23,24] has been verified by experiments [25–30].

The existence of the NLS has been proposed in Bernal graphite [31,32] and other all-carbon allotropes, including hyperhoneycomb lattices [33] and the Mackay-Terrones crystal (MTC) [12]. In Ref. [12], it was discussed that when spin-orbit coupling (SOC) is neglected and band inversion happens, the coexistence of time-reversal and inversion symmetry protects the NLS in 3D momentum space. It is heuristic that compounds with a light element can also exhibit nontrivial topology, which is totally different from the common wisdom that strong SOC in heavy-element compounds is crucial for topological quantum states. The NLS state was also proposed in photonic systems with time-reversal and inversion symmetry [34]. It was also shown that mirror symmetry, instead of inversion symmetry, together with time-reversal symmetry protects the NLS when SOC is neglected [35,36]. TaAs [23], Ca_3P_2 [37], and LaX (X = N, P, As, Sb, Bi) [38] belong to this type.

In the present work, based on first-principles calculations and effective model analysis, we demonstrate that the antiperovskite Cu_3PdN is a new candidate for realizing the NLS and drumheadlike surface flat bands [12,39–43], which may open an important route to achieving high-temperature superconductivity [44–46]. Strong SOC will drive the NLS in Cu_3PdN into a Dirac semimetal state with three pairs of Dirac points, leading to exotic surface Fermi arcs which can be observed on various surfaces of this material. This is very unique since the Dirac semimetals known so far, Na_3Bi and Cd_3As_2, have only one pair of Dirac points. When the C_4 crystal symmetry in Cu_3PdN is broken, the Dirac points are gapped and the system becomes a strong TI with Z_2 indices (1;111). It is well known that the cooperative interactions among lattice, charge, and spin degrees of freedom make antiperovskites

exhibit a wide range of interesting physical properties, such as superconductivity [47], giant magnetoresistance [48], negative thermal expansion [49], and magnetocaloric effect [50]. Our prediction of a 3D NLS and Dirac semimetal state in antiperovskites provides a promising platform for manipulating these exotic properties in the presence of nontrivial topology.

Crystal structure and methodology.—Perovskite has a formula ABX_3, where A and B are cations and X is an anion. The antiperovskite is similar to perovskite but switching the position of anion and cation, namely, in ABX_3 X stands for an electropositive cation, while A for an anion as shown in Fig. 1(a) for Cu_3PdN. Here we perform density functional calculations by using the Vienna *ab initio* simulation package [51] with generalized gradient approximation [52] and the projector augmented-wave method [53]. The surface band structures are calculated in a tight-binding scheme based on the maximally localized Wannier functions (MLWFs) [54], which are projected from the bulk Bloch wave functions.

Electronic structures.—The band structure of Cu_3PdN is shown in Fig. 2. The fat-band structure calculations suggest that the valence and conduction bands are dominated by Pd $4d$ (blue) and Pd $5p$ (red) states. They also indicate band inversion at R point, where the Pd $5p$ is lower than Pd $4d$ by about 1.5 eV. To overcome possible overestimation of band inversion [55], we employ hybrid density functionals [56] to confirm the existence of band inversion, while the energy gap at R point is slightly reduced to 1.1 eV.

Without SOC the occupied and unoccupied low energy bands are triply degenerate at the R point (six-fold degenerate if spin is considered). These states belong to the 3D irreducible representations Γ_4^- and Γ_5^+ of the O_h group at the R point, respectively. We emphasize that, unlike the situation in a typical TI such as the Bi_2Se_3 family compounds [57], the band inversion in Cu_3PdN is not due to SOC. To illustrate the band inversion process in Cu_3PdN explicitly, we calculated energy levels of Γ_5^+ and Γ_4^- bands at the R point for Cu_3PdN under different hydrostatic strains. As presented in Fig. 2(b), the band inversion happens at $a = 1.11a_0$ and the inversion energy increases when further compressing the lattice. The intriguing point of the Cu_3PdN band structure without SOC is that the band crossings due to the band inversion form a node-line circle because of the coexistence of time-reversal and inversion symmetry as addressed in Ref. [12].

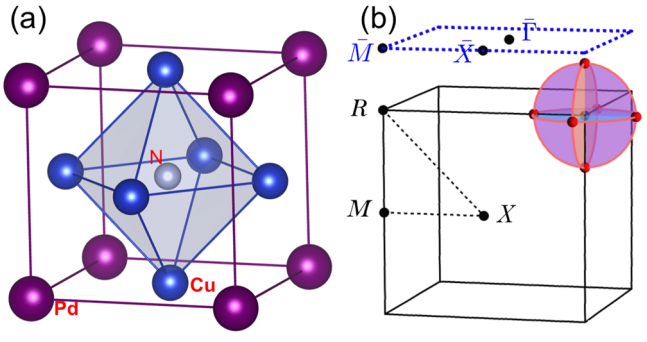

FIG. 1 (color online). (a) Crystal structure of antiperovskite Cu_3PdN with $Pm\bar{3}m$ (No. 221) symmetry. A nitrogen atom is at the center of the cube and is surrounded by octahedral Cu atoms. Pd is located at the corner of the cube. (b) Bulk and projected (001) surface Brillouin zone. The three node-line rings (orange) and three pairs of Dirac points (red), without and with SOC included, respectively, are schematically shown.

The protection of a node line can be inferred from the topological number of the form [39–43]

$$\gamma = \oint_C \mathcal{A}(\mathbf{k}) \cdot d\mathbf{k}, \tag{1}$$

where $\mathcal{A}(\mathbf{k})$ is the Berry connection of the occupied states, C is a closed loop in the momentum space. If C is pierced by the node line, one has $\gamma = \pi$, otherwise $\gamma = 0$. Below we prove the existence of the node line from the argument of codimension. A general 2×2 Hamiltonian is enough for describing the two crossing bands,

$$H(\mathbf{k}) = g_x(\mathbf{k})\sigma_x + g_y(\mathbf{k})\sigma_y + g_z(\mathbf{k})\sigma_z, \tag{2}$$

where $\mathbf{k} = (k_x, k_y, k_z)$, $g_{x,y,z}(\mathbf{k})$ are real functions and $\sigma_{x,y,z}$ are Pauli matrices characterizing the space of the two crossing bands, which are mainly from p_z and d_{xy} orbitals of Pd in Cu_3PdN. The coexistence of time-reversal and inversion symmetry leads to $g_y = 0$, g_x and g_z being odd and even functions of $\mathbf{k}$ [12]. Up to the lowest order of $\mathbf{k}$, $g_x(\mathbf{k})$ and $g_z(\mathbf{k})$ are given as

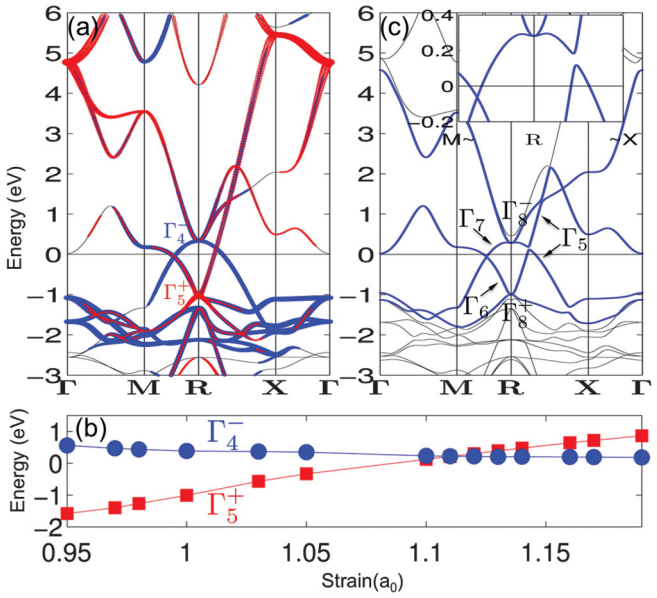

FIG. 2 (color). (a) Electronic band structure without SOC, where the component of Pd $5p$ ($4d$) orbitals is proportional to the width of the red (blue) curves. Band inversion between p and d orbits happens at the R point. (b) Evolution of energy levels of Γ_5^+ and Γ_4^- at R under hydrostatic pressure. Band inversion happens when $a < 1.11a_0$. (c) Electronic band structure with SOC included. A small gap is opened in the R-X direction while the Dirac point in the R-M direction is stable and protected by crystal symmetry C_4 rotation.

$$g_x(\mathbf{k}) = \gamma k_x k_y k_z, \tag{3}$$

$$g_z(\mathbf{k}) = M - B(k_x^2 + k_y^2 + k_z^2), \tag{4}$$

considering the crystal symmetry at the R point. The eigenvalues of Eq. (2) are $E(\mathbf{k}) = \pm\sqrt{g_x^2(\mathbf{k}) + g_z^2(\mathbf{k})}$. Node lines appear when $g_x(\mathbf{k}) = 0$ and $g_z(\mathbf{k}) = 0$. It is easy to check that $g_z(\mathbf{k}) = 0$ can be satisfied only in the case of $MB > 0$, which is nothing but the band inversion condition. When band inversion happens, there always exists three closed node lines in momentum space as shown in Fig. 1(b) which are the solutions of $g_x(\mathbf{k}) = g_z(\mathbf{k}) = 0$.

When SOC is considered, the six-fold degenerate states at R are split into one fourfold and one twofold degenerate state. As shown in Fig. 2(c), there are two fourfold degenerate states close to the Fermi energy: the occupied one with Γ_8^+ symmetry and the unoccupied one with Γ_8^- symmetry. Moving from R to X, the symmetry is lowered to C_{2v}. The fourfold degenerate states at R are split into twofold degenerate states along the R-X direction. The first-principles calculation shows that two sets of bands with the same Γ_5 symmetry are close to the Fermi energy and a gap ~0.062 eV is opened at the intersection as shown in the inset of Fig. 2(c). In order to reduce this SOC splitting and thus achieving the NLS, one can replace Pd with lighter elements, such as Ag and Ni. Along the R-M direction, the symmetry is characterized by the C_{4v} double group. As indicated in Fig. 2(c), the two sets of bands close to the Fermi energy belong to the Γ_7 and Γ_6 representation, respectively. They are decoupled and the crossing point on the R-M path is unaffected by SOC. They form a Dirac node near the Fermi energy as shown in Fig. 2(c), which is protected by the crystal symmetry C_4 rotation [4,10,58]. Once the C_4 rotational symmetry is broken, the Dirac node will be gapped, and the parities of the occupied states at eight time-reversal invariant momenta (TRIM) point are shown in Table. I. The Z_2 indices are (1;111), indicating a strong TI. The band structure of Cu_3PdN is different from that of antiperovskite Sr_3PbO [59,60], where the band inversion happens at Γ point and the involved bands belong to the same irreducible presentation, which leads to anti-crossing along the Γ-X direction.

Effective Hamiltonian for the 3D Dirac fermions.—In order to better understand the band crossing and gap opening discussed above, we derive a low energy effective Hamiltonian based on the theory of invariants in a similar way as that for the Bi_2Se_3 family [57].

We first construct the model Hamiltonian along the R-M direction parallel to the k_z axis. The symmetrical operations in this direction contain the crystalline C_{4v} symmetry and inversion with parity–time-reversal (PT) symmetry. As discussed above, the wave functions of low-energy states along the R-M direction are Γ_6 symmetry with angular momentum $j_z = \pm 1/2$ and Γ_7 with $j_z = \pm 3/2$. Therefore, the model Hamiltonian respecting both C_{4v} and PT symmetries can be written as

$$H_{RM} = \begin{bmatrix} \mathcal{M}_1 & 0 & c_2 k_+ & c_3 k_-^2 + c_4 k_+^2 \\ & \mathcal{M}_1 & c_4 k_-^2 + c_3 k_+^2 & -c_2 k_- \\ & & \mathcal{M}_2 & 0 \\ \dagger & & & \mathcal{M}_2 \end{bmatrix} \tag{5}$$

up to the second order of $\mathbf{k}$ in the basis of $\{|j_z = \frac{1}{2}\rangle_p, |j_z = -\frac{1}{2}\rangle_p, |j_z = \frac{3}{2}\rangle_d, |j_z = -\frac{3}{2}\rangle_d\}$, where $\mathcal{M}_1 = m_p + m_{11}k_z + m_{12}k^2$, $\mathcal{M}_2 = m_d + m_{21}k_z + m_{22}k^2$, $k^2 = k_x^2 + k_y^2 + k_z^2$ and $k_\pm = k_x \pm ik_y$. The C_4 rotation symmetry requires the matrix element between $|j_z = \frac{1}{2}\rangle$ and $|j_z = -\frac{3}{2}\rangle$ to take the form of $k_\pm^2$ in order to conserve the total angular moment along the z direction. Because of PT symmetry and mirror symmetry, all parameters in Eq. (5) can be chosen as real. Their values can be derived by fitting the dispersions to those of first-principles calculations [61].

On the k_z axis, the effective Hamiltonian is diagonal and the $|\pm 1/2\rangle$ sets and $|\pm 3/2\rangle$ sets are decoupled. Since the energies of p and d orbitals are inverted at the R point, namely, $m_p < m_d$ and $m_{22} < 0 < m_{12}$, the $|\pm 1/2\rangle$ and $|\pm 3/2\rangle$ bands cross at the $k_z^c = \{[(m_{11} - m_{21})^2 - 4(m_{12} - m_{22})(m_p - m_d)]^{1/2} - (m_{11} - m_{21})\}/[2(m_{12} - m_{22})]$ point.

The model Hamiltonian along the R-X direction can be derived in the same way with C_{2v} and PT symmetries. From the first-principles calculations, the states near the Fermi energy are characterized by Γ_5 with $j_z = |\pm 1/2\rangle$. The model Hamiltonian can be written as

$$H_{RX} = \begin{bmatrix} \mathcal{M}_1 & 0 & \mathcal{M}_3 & c_1 k_- \\ & \mathcal{M}_1 & c_1 k_+ & -\mathcal{M}_3 \\ & & \mathcal{M}_2 & 0 \\ \dagger & & & \mathcal{M}_2 \end{bmatrix} \tag{6}$$

up to the second order of $\mathbf{k}$ in the basis set of $\{|j_z = \frac{1}{2}\rangle_p, |j_z = -\frac{1}{2}\rangle_p, |j_z = \frac{1}{2}\rangle_d, |j_z = -\frac{1}{2}\rangle_d\}$. Here, k_z is set as along the R-X direction. The term $\mathcal{M}_3 = m_3 + m_{31}k_z + m_{32}k^2$ conserves the total angular momentum along the z direction. It couples the going-down Γ_5 states and going-up Γ_5 states and opens a gap at the crossing point shown in Fig. 2(c).

Surface states.—The band inversion and the 3D Dirac cones in Cu_3PdN suggest the presence of topologically nontrivial surface states. They are calculated based on the tight-binding Hamiltonian from the MLWF [5,54]. The obtained band structures and surface density of states (DOS) on semi-infinite (001) surface are presented in Fig. 3.

TABLE I. Parity product of occupied states at the TRIM points. The Z_2 indices are (1;111).

TRIM points	R	Γ	M (×3)	X (×3)
Parity product	+	−	−	−

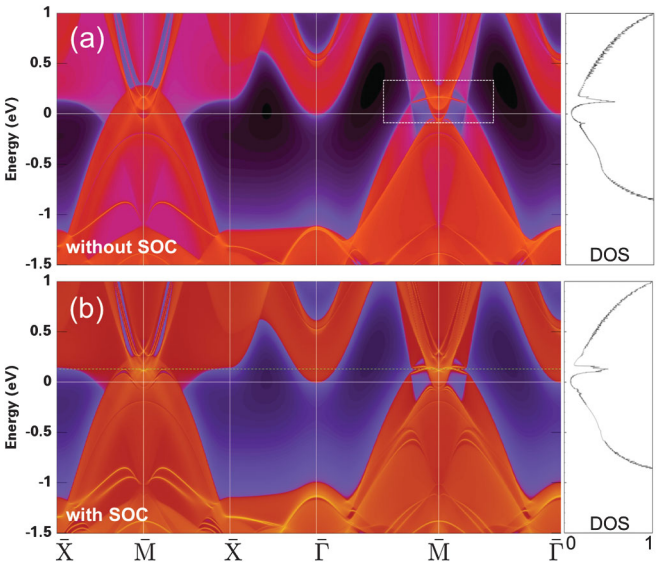

FIG. 3 (color). Band structures and DOS for (001) surface (a) without and (b) with SOC. Without SOC, the nearly flat surface bands are clearly shown in the white dashed box around the $\bar{M}$ point.

Without SOC, the bulk state is the same as the MTC [12] and there exists surface flat bands nestled inside the projected node-line ring on the (001) surface, namely, the "drumhead" states as shown in Figure 3(a). The peaklike DOS from these nearly flat bands is also clearly shown. The small dispersion of this drumhead state comes from the fact that the node-line ring is not necessarily on the same energy level due to the particle-hole asymmetry [11,12,46]. This result is consistent with the correspondence between the Dirac line in bulk and the flat band at the boundary as established in Refs. [39–41,43]. Such 2D flat bands and nearly infinite DOS are proposed as a route to achieving high-temperature superconductivity [44–46].

In the presence of SOC, the node-line ring will be gapped in general. However, there is an exception. For example, in the TaAs family each ring evolves into three pairs of Weyl nodes [23]. In Cu_3PdN, each ring is driven into one pair of Dirac nodes. The (001) surface state band structure in Fig. 3(b) clearly shows the gapped bulk state along the $\bar{\Gamma}$-$\bar{M}$ direction and the existence of a surface Dirac cone due to topologically nontrivial Z_2 indices as seen in Na_3Bi [4] and Cd_3As_2 [10]. The bulk band structure along R-X and R-M overlap each other when projected onto (001) surface along the $\bar{X}$-$\bar{M}$ path. The bulk Dirac cones are hidden by other bulk bands. Therefore, it is difficult to identify the detailed connection of Fermi arcs in the Fermi surface plot as shown in Fig. 4, though some eyebrowlike Fermi arcs can be clearly seen around these projected Dirac nodes.

Conclusion.—In summary, we propose that 3D topological node-line semimetal states can be obtained in a nonmagnetic and centrosymmetric system Cu_3PdN. The drumheadlike surface flat bands nestled in a projected node-line ring have been obtained. Including SOC will drive each node-line ring into one pair of Dirac points to host a Dirac semimetal state. The surface Dirac cone and

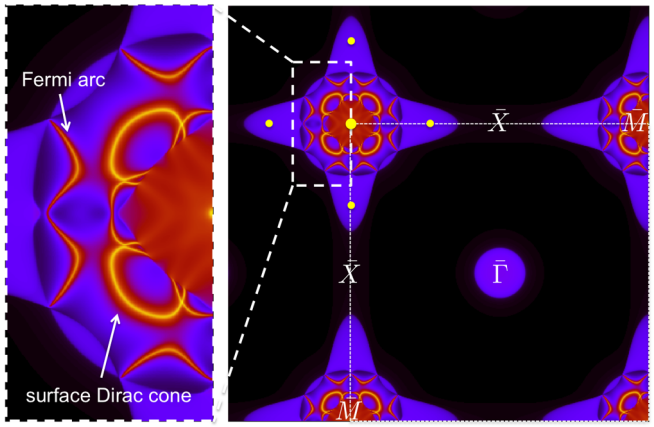

FIG. 4 (color online). Fermi surface of (001) surface shown in Fig. 3(b) with the chemical potential at 0.12 eV [green dashed line in Fig. 3(b)]. The yellow dots are projected Dirac points. The bigger one at $\bar{M}$ means that there are two Dirac points superposed there.

the Fermi arcs around the projected Dirac cones are observed. The existence of multiple pairs of 3D Dirac points distinguishes this system from other Dirac semimetals with only one pair. The cubic antiperovskite structure of Cu_3PdN makes it a good platform for manipulating ferromagnetism, ferroelectricity, and superconductivity realized in a broad class of materials with perovskite structure in the presence of nontrivial topology.

This work was supported by the WPI Initiative on Materials Nanoarchitectonics, and Grant-in-Aid for Scientific Research under the Innovative Area "Topological Quantum Phenomena" (No. 25103723), MEXT of Japan. H. M., Z. F., and X. D. were supported by the National Natural Science Foundation of China, the 973 Program of China (No. 2011CBA00108 and No. 2013CB921700), and the "Strategic Priority Research Program (B)" of the Chinese Academy of Sciences (No. XDB07020100).

Note added.—Recently, we became aware of a similar work by Kim *et al.* [62].

*hmweng@iphy.ac.cn
†Hu.Xiao@nims.go.jp

[1] M. Z. Hasan and C. L. Kane, Rev. Mod. Phys. **82**, 3045 (2010).
[2] X. L. Qi and S.-C. Zhang, Rev. Mod. Phys. **83**, 1057 (2011).
[3] P. Hořava, Phys. Rev. Lett. **95**, 016405 (2005).
[4] Z. Wang, Y. Sun, X.-Q. Chen, C. Franchini, G. Xu, H. Weng, X. Dai, and Z. Fang, Phys. Rev. B **85**, 195320 (2012).
[5] H. Weng, X. Dai, and Z. Fang, MRS Bull. **39**, 849 (2014).
[6] H. B. Nielsen and M. Ninomiya, Phys. Lett. **130B**, 389 (1983).
[7] X. Wan, A. M. Turner, A. Vishwanath, and S. Y. Savrasov, Phys. Rev. B **83**, 205101 (2011).
[8] G. Xu, H. Weng, Z. Wang, X. Dai, and Z. Fang, Phys. Rev. Lett. **107**, 186806 (2011).

[9] L. Balents, Physics **4**, 36 (2011).
[10] Z. Wang, H. Weng, Q. Wu, X. Dai, and Z. Fang, Phys. Rev. B **88**, 125427 (2013).
[11] A. A. Burkov, M. D. Hook, and L. Balents, Phys. Rev. B **84**, 235126 (2011).
[12] H. Weng, Y. Liang, Q. Xu, R. Yu, Z. Fang, X. Dai, and Y. Kawazoe, Phys. Rev. B **92**, 045108 (2015).
[13] B.-J. Yang and N. Nagaosa, Nat. Commun. **5**, 4898 (2014).
[14] Z. K. Liu, B. Zhou, Y. Zhang, Z. J. Wang, H. M. Weng, D. Prabhakaran, S.-K. Mo, Z. X. Shen, Z. Fang, X. Dai, Z. Hussain, and Y. L. Chen, Science **343**, 864 (2014).
[15] Z. K. Liu, J. Jiang, B. Zhou, Z. J. Wang, Y. Zhang, H. M. Weng, D. Prabhakaran, S.-K. Mo, H. Peng, P. Dudin, T. Kim, M. Hoesch, Z. Fang, X. Dai, Z. X. Shen, D. L. Feng, Z. Hussain, and Y. L. Chen, Nat. Mater. **13**, 677 (2014).
[16] M. Neupane, S.-Y. Xu, R. Sankar, N. Alidoust, G. Bian, C. Liu, I. Belopolski, T.-R. Chang, H.-T. Jeng, H. Lin, A. Bansil, F. Chou, and M. Z. Hasan, Nat. Commun. **5**, 3786 (2014).
[17] S. Jeon, B. B. Zhou, A. Gyenis, B. E. Feldman, I. Kimchi, A. C. Potter, Q. D. Gibson, R. J. Cava, A. Vishwanath, and A. Yazdani, Nat. Mater. **13**, 851 (2014).
[18] A. A. Zyuzin, S. Wu, and A. A. Burkov, Phys. Rev. B **85**, 165110 (2012).
[19] G. B. Halász and L. Balents, Phys. Rev. B **85**, 035103 (2012).
[20] M. Hirayama, R. Okugawa, S. Ishibashi, S. Murakami, and T. Miyake, Phys. Rev. Lett. **114**, 206401 (2015).
[21] J. Liu and D. Vanderbilt, Phys. Rev. B **90**, 155316 (2014).
[22] S. Murakami, New J. Phys. **9**, 356 (2007).
[23] H. Weng, C. Fang, Z. Fang, B. A. Bernevig, and X. Dai, Phys. Rev. X **5**, 011029 (2015).
[24] S.-M. Huang, S.-Y. Xu, I. Belopolski, C.-C. Lee, G. Chang, B. Wang, N. Alidoust, G. Bian, M. Neupane, A. Bansil, H. Lin, and M. Z. Hasan, arXiv:1501.00755v1.
[25] B. Q. Lv, H. M. Weng, B. B. Fu, X. P. Wang, H. Miao, J. Ma, P. Richard, X. C. Huang, L. X. Zhao, G. F. Chen, Z. Fang, X. Dai, T. Qian, and H. Ding, arXiv:1502.04684v1.
[26] B. Q. Lv, N. Xu, H. M. Weng, J. Z. Ma, P. Richard, X. C. Huang, L. X. Zhao, G. F. Chen, C. Matt, F. Bisti, V. Strokov, J. Mesot, Z. Fang, X. Dai, T. Qian, M. Shi, and H. Ding, arXiv:1503.09188.
[27] X. C. Huang, L. X. Zhao, Y. J. Long, P. P. Wang, D. Chen, Z. H. Yang, H. Liang, M. Q. Xue, H. M. Weng, Z. Fang, X. Dai, and G. F. Chen, arXiv:1503.01304.
[28] S.-Y. Xu, I. Belopolski, N. Alidoust, M. Neupane, C. Zhang, R. Sankar, S.-M. Huang, C.-C. Lee, G. Chang, B. Wang, G. Bian, H. Zheng, D. S. Sanchez, F. Chou, H. Lin, S. Jia, and M. Z. Hasan, arXiv:1502.03807v1.
[29] C. Shekhar, A. K. Nayak, Y. Sun, M. Schmidt, M. Nicklas, I. Leermakers, U. Zeitler, W. Schnelle, J. Grin, C. Felser, and B. Yan, arXiv:1502.04361v1.
[30] S.-Y. Xu, N. Alidoust, I. Belopolski, C. Zhang, G. Bian, T.-R. Chang, H. Zheng, V. Strokov, D. S. Sanchez, G. Chang, Z. Yuan, D. Mou, Y. Wu, L. Huang, C.-C. Lee, S.-M. Huang, B. Wang, A. Bansil, H.-T. Jeng, T. Neupert, A. Kaminski, H. Lin, S. Jia, and M. Z. Hasan, arXiv:1504.01350.
[31] G. P. Mikitik and Y. V. Sharlai, Phys. Rev. B **73**, 235112 (2006).
[32] G. P. Mikitik and Y. V. Sharlai, Low Temp. Phys. **34**, 794 (2008).
[33] K. Mullen, B. Uchoa, and D. T. Glatzhofer, Phys. Rev. Lett. **115**, 026403 (2015).
[34] L. Lu, L. Fu, J. D. Joannopoulos, and M. Soljačić, Nat. Photonics **7**, 294 (2013).
[35] C.-K. Chiu and A. P. Schnyder, Phys. Rev. B **90**, 205136 (2014).
[36] S. A. Yang, H. Pan, and F. Zhang, Phys. Rev. Lett. **113**, 046401 (2014).
[37] L. S. Xie, L. M. Schoop, E. M. Seibel, Q. D. Gibson, W. Xie, and R. J. Cava, arXiv:1504.01731.
[38] M. Zeng, C. Fang, G. Chang, Y.-A. Chen, T. Hsieh, A. Bansil, H. Lin, and L. Fu, arXiv:1504.03492.
[39] S. Ryu and Y. Hatsugai, Phys. Rev. Lett. **89**, 077002 (2002).
[40] T. T. Heikkilä, N. B. Kopnin, and G. E. Volovik, JETP Lett. **94**, 233 (2011).
[41] T. T. Heikkilä and G. E. Volovik, JETP Lett. **93**, 59 (2011).
[42] T. T. Heikkilä and G. E. Volovik, arXiv:1505.03277.
[43] G. E. Volovik, Lect. Notes Phys. **870**, 343 (2013).
[44] N. B. Kopnin, T. T. Heikkilä, and G. E. Volovik, Phys. Rev. B **83**, 220503 (2011).
[45] G. E. Volovik, arXiv:1409.3944.
[46] T. T. Heikkila and G. E. Volovik, arXiv:1504.05824.
[47] T. He, Q. Huang, A. P. Ramirez, Y. Wang, K. A. Regan, N. Rogado, M. A. Hayward, M. K. Haas, J. S. Slusky, K. Inumara, H. W. Zandbergen, N. P. Ong, and R. J. Cava, Nature (London) **411**, 54 (2001).
[48] H. Tashiro, R. Suzuki, T. Miyawaki, K. Ueda, and H. Asano, J. Korean Phys. Soc. **63**, 299 (2013).
[49] K. Takenaka and H. Takagi, Appl. Phys. Lett. **87**, 261902 (2005).
[50] B. S. Wang, P. Tong, Y. P. Sun, X. B. Zhu, X. Luo, G. Li, W. H. Song, Z. R. Yang, and J. M. Dai, J. Appl. Phys. **105**, 083907 (2009).
[51] G. Kresse and J. Furthmüller, Phys. Rev. B **54**, 11169 (1996).
[52] J. P. Perdew, K. Burke, and M. Ernzerhof, Phys. Rev. Lett. **77**, 3865 (1996).
[53] P. E. Blöchl, Phys. Rev. B **50**, 17953 (1994).
[54] N. Marzari, A. A. Mostofi, J. R. Yates, I. Souza, and D. Vanderbilt, Rev. Mod. Phys. **84**, 1419 (2012).
[55] J. Vidal, X. Zhang, L. Yu, J.-W. Luo, and A. Zunger, Phys. Rev. B **84**, 041109 (2011).
[56] J. Heyd, G. E. Scuseria, and M. Ernzerhof, J. Chem. Phys. **118**, 8207 (2003).
[57] H. Zhang, C.-X. Liu, X. L. Qi, X. Dai, Z. Fang, and S.-C. Zhang, Nat. Phys. **5**, 438 (2009).
[58] X.-L. Sheng, Z. Wang, R. Yu, H. Weng, Z. Fang, and X. Dai, Phys. Rev. B **90**, 245308 (2014).
[59] T. H. Hsieh, J. Liu, and L. Fu, Phys. Rev. B **90**, 081112 (2014).
[60] T. Kariyado and M. Ogata, J. Phys. Soc. Jpn. **81**, 064701 (2012).
[61] The fitted parameters are listed: $m_p = -1.12$ eV, $m_d = 0.254$ eV, $m_{11} = -0.86$, $m_{12} = 33.6$, $m_{21} = -0.40$, $m_{22} = -7.1$, $m_3 = 0.1$, $m_{31} = 0.51$, $m_{32} = -3.1$, $c_1 = 0.3$, $c_2 = -0.2$, $c_3 = 1.2$, and $c_4 = 0.95$, where the unit of energy is eV and the unit of length is the lattice constant.
[62] Y. Kim, B. J. Wieder, C. L. Kane, and A. M. Rappe, preceding Letter, Phys. Rev. Lett. **115**, 036806 (2015).